Robust Optimal Control of Nonlinear Systems via Homotopy Shooting Method

Adrian Stein and Tarunraj Singh

Abstract—This paper introduces an algorithm for solving robust optimal controllers for nonlinear systems using the homotopy shooting method. Robustness is ensured by penalizing the sensitivity states of the models during the transition and at the final time. In two examples, the cost is represented by the tracking error and terminal residual energy for a rest-to-rest maneuver. The proposed approach is illustrated on a double mass-spring-damper system and on a Type 1 Diabetes model where the cost function includes the integral of the tracking error. Our method can be readily extended for de-sensitization of multiple states over the whole time interval.

Index Terms—Optimal Control, Numerical Methods, Homotopy, Robustness.

I. INTRODUCTION

For many optimal control problems in engineering applications, it is burdensome to derive analytical or closed form solutions using Pontryagin's maximum principle [1]. Explicitly, posing the optimal control problem as a two-pointboundary-value problem leads to difficulty in obtaining the optimal solution due to the sensitivity of convergence to the initial guesses [2][3]. One approach to tackle this problem is to use iterative/numerical methods, for instance, continuation methods [4]. Homotopy falls in the category of continuation methods by tracking a zero-curve [5]. The main motivation is to start by solving an easy problem and slowly transforming the system to the complex problem of interest [1]. Thus, the homotopy parameter is used to blend the convex combination of the simple and complex system while being iteratively incremented. The previous homotopy step's solution is used as an initial guess for the next homotopy step [1].

The homotopy perturbation method has been used in conjunction with the Padé approximation to solve the Hamilton–Jacobi–Bellman equation [6], and to maximize the wind energy capture and reducing the mechanical stress on the drive train [7]. Work [1] illustrated a numerical example of a three-dimensional orbit transfer problem for a spacecraft with a single shooting homotopy method. Their homotopy was exploited between a linear system and a nonlinear system and neighboring extremal optimal control where constraints were applied to the input as well. Work [8] has used optimal homotopy asymptotic method to find the optimal solutions of fractional order of fuzzy differential equations. Work [9] linked convex programming and homotopy for a fuel-optimal low-thrust trajectory optimization problem.

A. Stein and T. Singh is with the Department of Mechanical and Aerospace Engineering, University at Buffalo, NY 14260, USA. (email: {astein3,tsingh}@buffalo.edu).

They transitioned the homotopic path from the minimumenergy to the minimum fuel, which can be used in deepspace cruise, where robustness and convergence are more important than optimality. Most homotopy approaches are applied in the aerospace community such as for generating an optimal open-loop large-angle 3-D maneuver for an asymmetric spacecraft for the case when one of the nominal maneuver actuators fails [10], rapid cooperative rendezvous problem between two spacecraft [11], solving for irregular asteroid landing [12], etc. In other domains, the homotopy approach has been used in the medical field for instance in the optimization in chemotherapy in cancer research [13]. It is well known that for certain problems a continuous zero-curve which in our case translates the problem from the linear to nonlinear system might not exist [2]. Recently approaches such as double-homotopy [2] or fractional homotopy [14] have been proposed to address this issue, where it was concluded that either there is a remaining feasibility dependent on the initial guess of the states or an immense computational burden. Another method presented by [15] involves 4 homotopy strategies for one problem to obtain multiple local solutions.

For our examples zero-curves exist. We choose two examples: 1) 2 spring-mass-damper system (floating oscillator) with a nonlinear spring as a benchmark example and 2) Type 1 Diabetes model. For the floating oscillator, the goal is to track the desired reference trajectory and simultaneously ensure robustness towards parameter uncertainties. The Type 1 Diabetes model is bilinear and we provide the optimal solution for a linearized version. Then, we show that posing the problem in a robust manner, the blood glucose level is desensitized towards a single parameter uncertainty. This paper will proceed as follows: In Section II we illustrate the methodology of our proposed homotopy shooting algorithm. In Section III, we describe the numerical results of the floating oscillator and Type 1 Diabetes model. In Section IV, we provide a brief conclusion.

II. METHODOLOGY

The proposed approach entails deriving the optimal solution in closed form for a linear system and transition that to a solution for the nonlinear system with a blending parameter λ . Consider the optimal control problem:

$$J=k(e(T),\lambda)+\int_0^TL(e(t),u(t),\lambda)dt$$
 s.t.:
$$\dot{x}=Ax+Bu+D(t)\quad x(0)=x_0 \tag{1}$$

$$e = (Cx - y_d). (2)$$

Define the Hamiltonian as:

$$\mathcal{H} = L(e(t), u(t), \lambda) + \psi^{T}(Ax + Bu + D(t)). \tag{3}$$

The costates are defined as:

$$\dot{\psi} = -\frac{\partial H}{\partial x} = -\frac{\partial L}{\partial x} - A^T \psi, \quad \psi(\tau) = \left. \frac{\partial e^T}{\partial x} \frac{\partial k}{\partial e} \right|_T$$
 (4)

$$\frac{\partial H}{\partial u} = \frac{\partial L}{\partial u} + B^{\mathsf{T}} \psi = 0 \quad (5)$$

For a quadratic cost function of a tracking problem, the problem reduces to:

$$J = \frac{1}{2}e^{T}Q_{f}e(T) + \frac{1}{2}\int_{0}^{T} (e(t)^{T}Qe(t) + u^{T}Ru) dt \quad (6)$$

$$H = \frac{1}{2}e^{T}Qe + \frac{1}{2}u^{T}Ru + \psi^{T}(Ax + Bu + D(t))$$
 (7)

$$\dot{\psi} = -C^T Q \left(Cx - y_d \right) - A^T \psi \quad (8)$$

$$\frac{\partial H}{\partial u} = Ru + B^{\mathsf{T}} \psi = 0 \quad \Rightarrow \quad u = -R^{-1} B^{\mathsf{T}} \psi. \quad (9)$$

The state and costate derivatives are:

$$\dot{x} = Ax - BR^{-1}B^T\psi + D(t) \tag{10}$$

$$\dot{\psi} = -C^T Q C x - A^T \psi + C^T Q y_d, \tag{11}$$

which can be rewritten as:

$$\begin{bmatrix} \dot{x} \\ \dot{\psi} \end{bmatrix} = \underbrace{\begin{bmatrix} A & -BR^{-1}B^T \\ -C^TQC & -A^T \end{bmatrix}}_{A} \begin{bmatrix} x \\ \psi \end{bmatrix} + \underbrace{\begin{bmatrix} D(t) \\ C^TQy_d \end{bmatrix}}_{B}. \quad (12)$$

The solution to this equation is:

$$\begin{bmatrix} x \\ \psi \end{bmatrix} (T) = e^{\mathcal{A}T} \begin{bmatrix} x \\ \psi \end{bmatrix} (0) + \int_0^T e^{\mathcal{A}(T-\tau)} \mathcal{B}(\tau) d\tau, \quad (13)$$

which can be represented as:

$$\begin{bmatrix} x \\ \psi \end{bmatrix} (T) = \begin{bmatrix} \phi_{11} & \phi_{12} \\ \phi_{21} & \phi_{22} \end{bmatrix} \begin{bmatrix} x \\ \psi \end{bmatrix} (0) + \begin{bmatrix} \Gamma_1 \\ \Gamma_2 \end{bmatrix}. \tag{14}$$

Since the transversality conditions require:

$$\psi(T) = C^T Q_f \left(Cx(T) - y_d(T) \right), \tag{15}$$

we have:

$$\phi_{21}x(0) + \phi_{22}\psi(0) + \Gamma_2 =$$

$$C^{T}Q_{f}\left(C\left(\phi_{11}x(0)+\phi_{12}\psi(0)+\Gamma_{1}\right)-y_{d}(T)\right),$$
 (16)

which leads to the solution:

$$(\phi_{22} - C^T Q_f C \phi_{12}) \psi(0) = (C^T Q_f C \phi_{11} - \phi_{21}) x(0) + C^T Q_f (C \Gamma_1 - y_d(T)) - \Gamma_2$$
(17)

$$\leftrightarrow \psi(0) = (\phi_{22} - C^T Q_f C \phi_{12})^{-1} ((C^T Q_f C \phi_{11} - \phi_{21}) x(0) + C^T Q_f (C \Gamma_1 - y_d(T)) - \Gamma_2),$$
(18)

which can be used to generate the optimal state, costates and control which serve as the initial solution for the homotopy loop. This solution corresponds to the optimal solution for the homotopy parameter $\lambda=0$. The homotopy optimal control problem is posed as:

$$J = \frac{1}{2}e^{T}(T)Q_{f}e(T)(1-\lambda) + \lambda\phi(x(T))$$
$$+ \frac{1}{2}\int_{0}^{T} (1-\lambda)\left(e^{T}(t)Qe(t) + u(t)^{T}Ru(t)\right)$$
$$+ \lambda L(x(t), u(t)) dt \tag{19}$$

s.t.:
$$\dot{x} = (1 - \lambda) (Ax(t) + Bu(t) + D(t))$$

 $+ \lambda (f(x(t), u(t))) = F(x(t), u(t), \lambda).$ (20)

Define the Hamiltonian as:

$$H = \frac{1}{2}(1 - \lambda)\left[e^T Q e + u^T R u\right] + \lambda L + \psi^T F, \qquad (21)$$

which leads to the necessary conditions for optimality:

$$\dot{\psi} = -H_x = -(1 - \lambda)C^T Q e - \lambda \frac{\partial L}{\partial x} - \frac{\partial F^T}{\partial x} \psi, \quad (22)$$

where $e(t) = Cx(t) - y_d(t)$. The transversality conditions leads to:

$$\psi(T) = (1 - \lambda)C^T Q_f e(T) + \lambda \phi_x(T), \qquad (23)$$

and the optimal control is derived from:

$$\frac{\partial H}{\partial u} = 0 \Rightarrow (1 - \lambda)Ru + \lambda \frac{\partial L}{\partial u} + \frac{\partial F^T}{\partial u}\psi = 0, \quad (24)$$

which is solved for u(t) resulting in the equation:

$$u(t) = g(x(t), \psi(t), \lambda), \tag{25}$$

which results in the two point boundary value problem with the coupled state-costate equations:

$$\dot{x} = (1 - \lambda) \left[Ax + B(x, \psi) + D(t) \right]$$
$$+ \lambda f(x, g(x(t), \psi(t), \lambda))$$
(26)

$$\dot{\psi} = -(1 - \lambda)C^T Q e - \lambda \frac{\partial L}{\partial x} - \frac{\partial F^T}{\partial x} \psi, \qquad (27)$$

and the boundary constraints are $x(0)=x_0$ and $\psi(T)=(1-\lambda)C^TQ_fe(T)+\lambda\phi_x(T)$. The quasi-linearization approach to solve the boundary value problem requires the model being linearized about the nominal trajectory and is used to increment toward the optimal trajectory. For simplicity we introduce using the index $(.)_x$ and $(.)_{xx}$ to represent the first and second derivative with respect to the variable x, respectively. This notation holds for all other variable choices. The quasi-linearization approach leads to:

$$\delta \dot{x} = F_x \delta x + F_u \delta u + F_\lambda \delta \lambda \tag{28}$$

$$\delta \dot{\psi} = -H_{xx}\delta x - H_{xy}\delta u - H_{xy}\delta \psi - H_{x\lambda}\delta \lambda, \tag{29}$$

and the linearized optimality condition leads to the optimal perturbation control:

$$H_{ux}\delta x + H_{u\psi}\delta\psi + H_{uu}\delta u + H_{u\lambda}\delta\lambda = 0 \tag{30}$$

$$\rightarrow \delta u = -H_{uu}^{-1} \left[H_{ux} \delta x + H_{u\psi} \delta \psi + H_{u\lambda} \delta \lambda \right]. \tag{31}$$

The shooting method can now be used to solve for the perturbations in initial costates to satisfy the transversality conditions.

$$\delta \dot{x} = \left[F_{x} - F_{u} H_{uu}^{-1} H_{ux} \right] \delta_{x} + \left[-F_{u} H_{uu}^{-1} H_{u\psi} \right] \delta\psi + \left[F_{\lambda} - F_{u} H_{uu}^{-1} H_{u\lambda} \right] \delta\lambda \quad (32)$$
$$\delta \dot{\psi} = \left[-H_{xx} + H_{xu} H_{uu}^{-1} H_{ux} \right] \delta x + \left[-H_{x\psi} + H_{xu} H_{uu}^{-1} H_{u\psi} \right] \delta\psi + \left[-H_{x\lambda} + H_{xu} H_{uu}^{-1} H_{u\lambda} \right] \delta\lambda, \quad (33)$$

which can be written in a matrix-form as:

$$\begin{bmatrix} \delta \dot{x} \\ \delta \dot{\psi} \end{bmatrix} = \mathcal{A}^*(x^*, \psi^*) \begin{bmatrix} \delta x \\ \delta \psi \end{bmatrix} + \mathcal{B}^*(x^*, \psi^*) \delta \lambda \quad (34)$$

$$\mathcal{A}^*(x^*, \psi^*) =$$

$$\begin{bmatrix} F_x - F_u H_{uu}^{-1} H_{uu} & -F_u H_{uu}^{-1} H_{u\psi} \\ -H_{xx} + H_{xu} H_{uu}^{-1} H_{ux} & -H_{x\psi} + H_{xu} H_{uu}^{-1} H_{u\psi} \end{bmatrix}$$
(35)
$$\mathcal{B}^*(x^*, \psi^*) = \begin{bmatrix} F_\lambda - F_u H_{uu}^{-1} H_{u\lambda} \\ -H_{x\lambda} + H_{xu} H_{uu}^{-1} H_{u\lambda} \end{bmatrix},$$
(36)

$$\mathcal{B}^*(x^*, \psi^*) = \begin{bmatrix} F_{\lambda} - F_u H_{uu}^{-1} H_{u\lambda} \\ -H_{x\lambda} + H_{xu} H_{uu}^{-1} H_{u\lambda} \end{bmatrix}, \quad (36)$$

and we know that:

$$\psi(T) + \delta\psi(T) = (1 - \lambda) \left[C^T Q_f e(T) + C^T Q_f C \delta x(T) \right] + \lambda \left[\phi_x(T) + \phi_{xx} \delta x \right].$$
 (37)

The solution to this equation takes the form:

$$\begin{bmatrix} \delta x(T) \\ \delta \psi(T) \end{bmatrix} = e^{\mathcal{A}^* T} \begin{bmatrix} \delta x(0) \\ \delta \psi(0) \end{bmatrix} + \left(\int_0^T e^{\mathcal{A}^* (T - \tau)} \mathcal{B}^* (\tau) \, d\tau \right) \delta \lambda,$$
(38)

which can be represented as:

$$\begin{bmatrix} \delta x(T) \\ \delta \psi(T) \end{bmatrix} = \begin{bmatrix} \phi_{11}^* & \phi_{12}^* \\ \phi_{21}^* & \phi_{22}^* \end{bmatrix} \begin{bmatrix} \delta x(0) \\ \delta \psi(0) \end{bmatrix} + \begin{bmatrix} \Gamma_1^* \\ \Gamma_2^* \end{bmatrix} \delta \lambda. \tag{39}$$

Since A^* is time-varying, in order to identify ϕ_{11}^* , ϕ_{12}^* , ϕ_{21}^* and ϕ_{22}^* , the equation needs to be solved numerically with $\delta \lambda = 0$. Therefore, the initial conditions for $\delta x(0)$ and $\delta\psi(0)$ will be always unit-vectors starting with "1" at the first element while the last unit-vector has the "1" placed at the last element. In order to determine Γ_1^* and Γ_2^* , $\delta x(0)$ and $\delta\psi(0)$ will be set to **0** and $\delta\lambda\neq0$, where $\delta\lambda$ depends on the step size of the homotopy parameter. From the matrix form we can get:

$$\delta x(T) = \phi_{11}^* \delta x(0) + \phi_{12}^* \delta \psi(0) + \Gamma_1^* \delta \lambda \tag{40}$$

$$\delta\psi(T) = \phi_{21}^* \delta x(0) + \phi_{22}^* \delta \psi(0) + \Gamma_2^* \delta \lambda. \tag{41}$$

Since the transversality conditions require:

$$\psi(T) + \delta\psi(T) = C^T Q_f \underbrace{\left(Cx(T) - y_d(T)\right)}_{e(T)} + C^T Q_f C \delta x(T),$$
(42)

we have:

$$\psi(T) + \phi_{21}^* \delta x(0) + \phi_{22}^* \delta \psi(0) + \Gamma_2^* =$$

$$C^T Q_f e(T) + C^T Q_f C \left(\phi_{11}^* \delta x(0) + \phi_{12}^* \delta \psi(0) + \Gamma_1^* \right) \quad (43)$$

$$\phi_{22}^* \delta \psi(0) - C^T Q_f C \phi_{12}^* \delta \psi(0) =$$

$$C^T Q_f e(T) + C^T Q_f C \phi_{11}^* \delta x(0)$$

$$-\phi_{21}^* \delta x(0) + C^T Q_f C \Gamma_1^* - \Gamma_2^* - \psi(T), \quad (44)$$

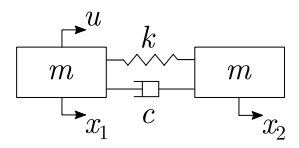


Fig. 1: Floating oscillator model.

which leads to the solution:

so that:

$$\psi(k+1) = \psi(k) + \delta\psi(0). \tag{46}$$

If the difference between $\psi(T)$ from the numerical integration and $\psi(T) = C^T Q_f (Cx(T) - y_d(T))$ is below a certain tolerance the homotopy parameter λ gets incremented.

III. RESULTS

The two examples in this work are the floating oscillator and the Type 1 Diabetes model. The sensitivity of the states to any model parameter is used to augment the state space model, which is presented in Section II to penalize the integral of the sensitivity states.

A. Floating Oscillator

Fig. 1 illustrates a double spring-mass-damper system, where the first and second masses are connected with a spring of stiffness k and a damper with a damping coefficient c. The equations of motion for the linear system are:

$$\ddot{x}_1 = -k(x_1 - x_2) - c(\dot{x}_1 - \dot{x}_2) + u \tag{47a}$$

$$\ddot{x}_2 = k(x_1 - x_2) + c(\dot{x}_1 - \dot{x}_2), \tag{47b}$$

while the counterpart nonlinear system is represented as:

$$\ddot{x}_1 = -k(x_1 - x_2)^3 - c(\dot{x}_1 - \dot{x}_2) + u \tag{48a}$$

$$\ddot{x}_2 = k(x_1 - x_2)^3 + c(\dot{x}_1 - \dot{x}_2). \tag{48b}$$

For the simulation we choose the elements m = 1, k = 1(nominal), c = 0.1, $Q_f = diag(100, 100, 100, 100)$, Q =diag(0, 10, 0, 0) and R = 1, where "diag" denotes the diagonal matrix. The number of increments for λ between 0 and 1 is 501 and the error tolerance is set to 0.1. The input only acts on the first mass while we enforce that the initial and final conditions are: $x_1(0) = \dot{x}_1(0) = x_2(0) = \dot{x}_2(0) = \dot{x}_2(0$ $x_1(t_f) = \dot{x}_1(t_f) = x_2(t_f) = \dot{x}_2(t_f) = 0$ where $t_f = 2\pi$. Additionally, we require the second mass to track a desired position of $x_{2,d} = 1 - \cos(t)$. We consider the sensitivity

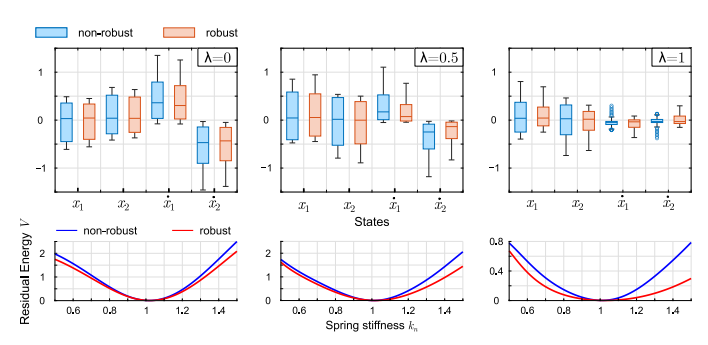


Fig. 2: Residual energy and position and velocity of the first and second mass for $\lambda = [0; 0.5; 1]$.

Fig. 3: Residual energy over uncertain $k \in [0.5, 1.5]$ with varying homotopy parameter $\lambda \in [0, 1]$.

states with respect to k as:

$$\frac{d\ddot{x}_{1}}{dk} = -x_{1} + x_{2} - k \left(\frac{dx_{1}}{dk} - \frac{dx_{2}}{dk}\right) - c \left(\frac{d\dot{x}_{1}}{dk} - \frac{d\dot{x}_{2}}{dk}\right) \tag{49a}$$

$$\frac{d\ddot{x}_{2}}{dk} = x_{1} - x_{2} + k \left(\frac{dx_{1}}{dk} - \frac{dx_{2}}{dk}\right) + c \left(\frac{d\dot{x}_{1}}{dk} - \frac{d\dot{x}_{2}}{dk}\right), \tag{49b}$$

whereas the nonlinear sensitivity states are:

$$\frac{d\ddot{x}_{1}}{dk} = -(x_{1} - x_{2})^{3}$$

$$-3k(x_{1} - x_{2})^{2} \left(\frac{dx_{1}}{dk} - \frac{dx_{2}}{dk}\right) - c\left(\frac{d\dot{x}_{1}}{dk} - \frac{d\dot{x}_{2}}{dk}\right)$$
(50a)
$$\frac{d\ddot{x}_{2}}{dk} = (x_{1} - x_{2})^{3}$$

$$+3k(x_{1} - x_{2})^{2} \left(\frac{dx_{1}}{dk} - \frac{dx_{2}}{dk}\right) + c\left(\frac{d\dot{x}_{1}}{dk} - \frac{d\dot{x}_{2}}{dk}\right).$$
(50b)

For the simulation with sensitivity states we choose the elements $Q_f = diag(100, 100, 100, 100, 0.4, 0.4, 0.4, 0.0)$ and Q =diag(0,10,0,0,0,0,0). We refer to the system defined by Eqs. (47)-(48) as nonrobust and Eqs. (49)-(50) as robust formulations. The residual energy at the final maneuver time t_f is defined as: $V(t_f) = \frac{1}{2}\dot{x}_1 + \frac{1}{2}\dot{x}_2 + \frac{1}{2}kx_1^2 + \frac{1}{2}k(x_2 - x_1)^2$. After we obtained the optimal control input u for the nonrobust and robust formulation, we simulate 61 different scenarios where k is equally spaced between 0.5 and 1.5. Fig. 2 shows the residual energy for cases of the homotopy parameter $\lambda = [0; 0.5; 1]$. On the lower panel it can be seen that penalizing the sensitivity states (robust formulation) is outperforming the nonrobust formulation, except around the nominal value both residual energies appear to be the same. The box whisker chart on the upper panel of Fig. 2 shows the quantity of each variable for $\lambda = [0; 0.5; 1]$. It can be seen that the robust solution brings the states closer to 0 compared to the nonrobust one. Fig. 3 illustrates the residual energy as a surface for all different homotopy stages of λ and uncertain variables k. This confirms that the residual energy V is smaller for the robust formulation during all homotopy stages compared to the nonrobust one. However, around the nominal value, the nonrobust solution is outperforming the robust one. Since putting weights on

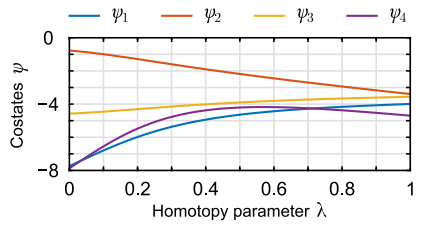


Fig. 4: Initial costates ψ over λ for the Floating Oscillator.

the sensitivity state is only a soft constraint, by changing the cost function it is possible that the nonrobust solution is superior in a close proximity of the nominal value of k=1, while for larger perturbations the robust solution is superior. The curvature plot of the residual energy with respect to k illustrates that around k = 1 for all λ the nonrobust case has a larger curvature meaning the residual energy is more sensitive to changes in k. The evolution of the initial costates can be seen in Fig. 4, where costate ψ_3 does not change a lot over the λ but ψ_1 , ψ_2 , and ψ_4 do. The change of the costates from the linear system to the nonlinear system is: $\psi_{linear} = [-7.7410, -0.7680, -4.5764, -7.8684]$ to $\psi_{nonlinear} = [-3.9901, -3.3921, -3.5619, -4.6975]$. To evaluate the importance of a good guess for the nonlinear system in order to ensure good tracking and satisfying the desired terminal states, we perturb the initial costate $\psi(0)$ as follows: $\psi(0) = \psi_{nonlinear}(0) + \epsilon [1, 1, 1, 1]$, where $\epsilon = [-0.5, 0.5]$ as 31 equally spaced increments. With these initial conditions we will try to derive the optimal solution while using the same cost as in the homotopy problem. The homotopy shooting algorithm took 501 iterations to converge at the optimal solution for $\lambda = 1$. Therefore, we constrain the pure shooting algorithm on the nonlinear system to maximal 501 iterations. If the algorithm converges to a solution we define the feasibility as 1 and 0 if it doesn't. The cost is described by Eqn. (6). Fig. 5 shows the feasibility, number of iterations and the cost J for a shooting algorithm on all perturbed initial costates. It can be seen that only for one case (very small perturbation) the cost is as good as for the homotopy approach, which shows the importance of good initial costates for an optimal control problem.

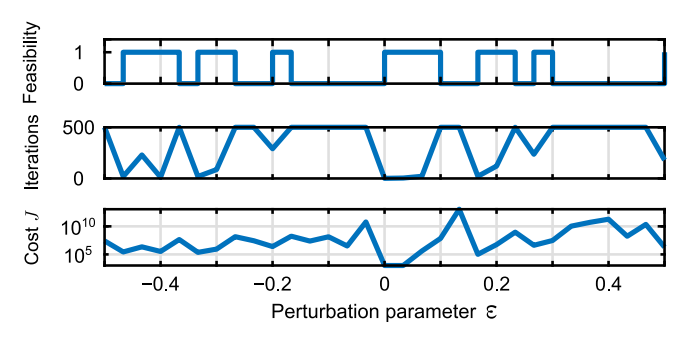


Fig. 5: Feasibility, number of iterations and cost for perturbed initial conditions of costates $\psi(0)$.

B. Minimal Bergman Diabetes Model

To illustrate our approach on another benchmark problem, we pick the Type 1 Diabetes problem. The minimal Bergman model [16][17], which is well established in the Diabetes research community is a third order nonlinear model:

$$\dot{G}(t) = -(X(t) + p_1)G(t) + p_1G_b + \frac{\mathcal{D}(t)}{V_a}$$
 (51a)

$$\dot{X}(t) = -p_2 X(t) + p_3 (I(t) - I_b)$$
 (51b)

$$\dot{I}(t) = -p_4 (I(t) - I_b) + U(t),$$
 (51c)

where G is the blood glucose level, X is the intermediate state and I is the insulin concentration. The variable $\mathcal{D}(t)$ is the meal disturbance term. In our case, the input U is unconstrained. The other values are given as follows: $p_1=0.0287$, $p_2=0.0283$, $p_3=5.035e-5$, $p_4=5/54$, and $I_b=15.3875$, which is the basal insulin level which is produced by the pancreas constantly. G_b the basal glucose concentration is assumed to be 119.1858. V_g is the distribution volume to insulin and is set to 128.8237. The goal is to track a desired blood glucose level G_{ref} over 50 minutes, so that the patient is not running into hypo- or hyperglycemia, both detrimental to the human body [18]. The minimal Bergman model is bilinear. For $\lambda=0$ we define variable G(t) as G_b and the system as:

$$A = \begin{bmatrix} 0 & -G_b & 0 \\ 0 & -p_2 & p_3 \\ 0 & 0 & -p_4 \end{bmatrix}; B = \begin{bmatrix} 0 \\ 0 \\ 1 \end{bmatrix}; C = I_3; D = \begin{bmatrix} \mathcal{D}(t) \\ -p_3 I_b \\ p_4 I_b \end{bmatrix},$$
(52)

which permits us to exploit the closed form shooting method on the system (see Eqs. (12)-(18)) and find the initial costates. I_3 is a 3×3 identity matrix. Fig. 6 shows that the blood glucose reference is rising steadily from 92 at 0 mins to 118.19 at 50 mins. Furthermore, the meal disturbance $\mathcal{D}(t)$ over t is shown. During the homotopy we apply a multiple shooting (one forward and one backward) method where the optimal control problem is split into two parts. We set the mid-time at 25 mins. The initial conditions are given as: $[G_0, X_0, I_0] = [92, 0, I_b]$ and the final state conditions derived from the closed form solution of the linear system are [118.4247, 0.0124, 17.8908]. The initial and final costates are: [-194.9168, 91805.4457, 3.7288] and

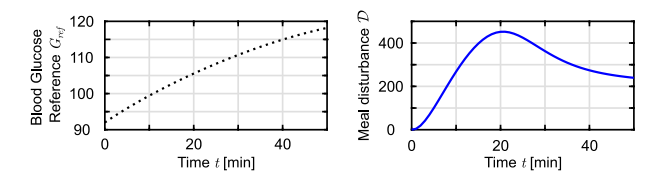


Fig. 6: Reference for the blood glucose level G_{ref} and meal disturbance $\mathcal{D}(t)$ over time.

[0.3849, -960.4652, 0.2694], respectively. The other parameters are given as $Q_f = diag\,(10,0,0)$, $Q = diag\,(10,0,0)$, and R = 1, and we choose 101 increments for changing λ from 0 to 1. The maximum error tolerance is set 0.1 and there are a maximum of 50 iterations per homotopy stage allowed.

We assume an uncertainty in the variable p_1 and add a sensitivity state for the blood glucose level to the Type 1 Diabetes model as:

$$\frac{d\dot{G}}{dp_1}(t) = -X(t)\frac{dG}{dp_1} - G(t) - p_1\frac{dG}{dp_1} + G_b.$$
 (53)

The goal is to derive a control input which minimizes the p_1 -sensitivity of the blood glucose level G and track G_{ref} well enough. To provide a fair comparison we set the sensitivity state $dG/dp_1(t_f)$ at final time of the the robust model to the same value as in the nonrobust model. Thus, $dG/dp_1(t_f)$ varies over λ . For the rest of the time the desired reference for the sensitivity state is 0 and we set $dG/dp_1(0) = 0$. Therefore, the initial and final states are: $[92, 0, I_b, 0]$ and $[118.4247, 0.0124, 17.8908, dG/dp_1(t_f, \lambda)]$. The initial and final costates are: [-239.1577, 118907.6007, 7.1911, 6.1970]and [1.4055, -0.0578, 1.4989e - 5, 0.0059], respectively. The cost function parameters are $Q_f = diag(10, 0, 0, 0.001)$ and Q = diag(10, 0, 0, 0.005). After deriving the optimal control input u for the nonrobust (original) and robust system we perturb p_1 between 0.0137 and 0.0437 in 31 equally spaced increments. This perturbation is 52.27% about the nominal value of p_1 . To compare the nonrobust and robust we propose analyzing the expected value (mean) and standard deviation of the blood glucose level. Fig. 7 illustrates the blood glucose reference trajectory (black dotted), the mean and standard deviation of the nonrobust (red) and robust (blue) solution for λ values of 0, 0.5 and 1, respectively. The mean of G shows that the tracking of the nonrobust solution is better than the robust one. Gaining robustness of a system output towards parameter uncertainty comes at a cost which is in this case tracking error. However, it can be concluded that the tracking error is small in both cases. The standard deviation is reduced for the robust control input compared to the nonrobust one. For $\lambda = 0$, it can be seen that there is no standard deviation, which is due to the absence of the parameter p_1 for the linear system (see Eqn. (52)). We compare the tracking error and standard deviation of the nonrobust and robust solution for all homotopy parameter stages λ and times t for an uncertainty

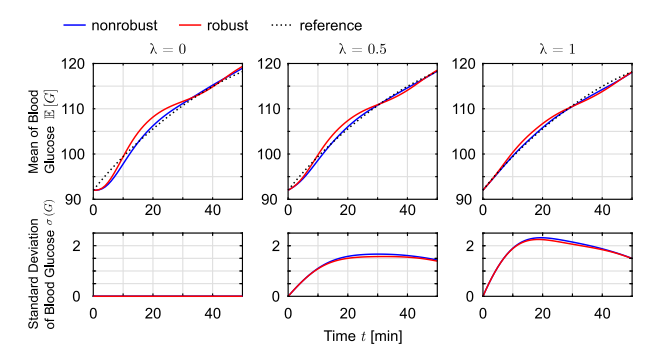


Fig. 7: Mean and standard deviation of blood glucose level G for non-robust and robust case for $\lambda = [0; 0.5; 1]$.

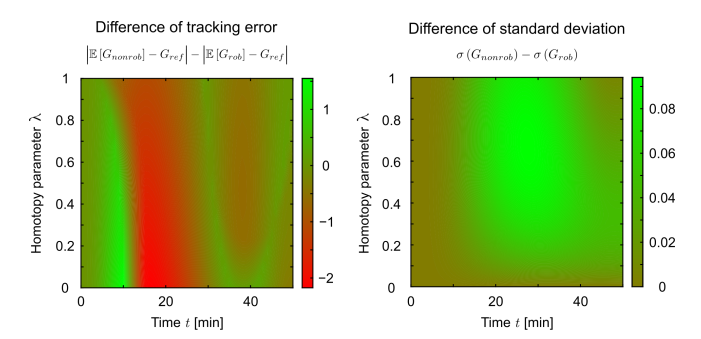


Fig. 8: Difference between absolute tracking error (left) and standard deviation (right) of nonrobust and robust solution.

in p_1 . Fig. 8 shows on the left the difference between the absolute tracking error of the nonrobust and robust solution. If the color is green then the tracking of robust solution is better than the nonrobust and if the color is red the tracking is worse. On the right side of Fig. 8, the difference of the standard deviation between the nonrobust and robust is shown, and the same color scheme applies. It can be seen that the tracking is better in certain instances for the robust formulation, while the nonrobust case delivers better tracking overall. The better measure to assess the sensitivity of the G with respect to p_1 is the standard deviation, where the robust solution is outperforming the nonrobust over the entire domain of uncertainty. This confirms that penalizing the sensitivity state actually desensitizes the controlled output to model parameter uncertainties.

IV. CONCLUSIONS

The methodology proposed in this study enables the derivation of an optimal control input for nonlinear systems while integrating robustness into the modeling process. We illustrated the applicability of this approach through two distinct cases: the well-known floating oscillator, serving as a benchmark, and a Type 1 Diabetes model designed for blood glucose tracking. Our results demonstrated the method's effectiveness with both single and multiple shooting techniques. It is important to note that there exists a trade-off between robustness and tracking performance. However, this trade-off minimally impacts tracking performance, and the

consistent reduction of standard deviation persists throughout the entire topological problem and time domain. Our future research will focus on imposing constraints on the control input while implementing the robust algorithm within the framework of the homotopy shooting method.

REFERENCES

- R. Gupta, A. M. Bloch, and I. V. Kolmanovsky, "Combined homotopy and neighboring extremal optimal control," *Optimal Control Applica*tions and Methods, vol. 38, no. 3, pp. 459–469, 2017.
- [2] B. Pan, P. Lu, X. Pan, and Y. Ma, "Double-homotopy method for solving optimal control problems," *Journal of Guidance, Control, and Dynamics*, vol. 39, no. 8, pp. 1706–1720, 2016.
- [3] M. Saghamanesh and H. Baoyin, "A robust homotopic approach for continuous variable low-thrust trajectory optimization," *Advances in Space Research*, vol. 62, no. 11, pp. 3095–3113, 2018.
- [4] F. A. Ficken, "The continuation method for functional equations," Communications on Pure and Applied Mathematics, vol. 4, no. 4, pp. 435–456, 1951.
- [5] X. Bai, J. Turner, and J. Junkins, 12th AIAA/ISSMO Multidisciplinary Analysis and Optimization Conference. [Reston, VA]: [American Institute of Aeronautics and Astronautics], 2008.
- [6] S. Ganjefar and S. Rezaei, "Modified homotopy perturbation method for optimal control problems using the padé approximant," *Applied Mathematical Modelling*, vol. 40, no. 15-16, pp. 7062–7081, 2016.
- [7] M. Abolvafaei and S. Ganjefar, "Maximum power extraction from wind energy system using homotopy singular perturbation and fast terminal sliding mode method," *Renewable Energy*, vol. 148, no. 2, pp. 611–626, 2020.
- [8] D. J. Hashim, A. F. Jameel, T. Y. Ying, A. K. Alomari, and N. R. Anakira, "Optimal homotopy asymptotic method for solving several models of first order fuzzy fractional ivps," *Alexandria Engineering Journal*, vol. 61, no. 6, pp. 4931–4943, 2022.
- [9] A. C. Morelli, C. Hofmann, and F. Topputo, "Robust low-thrust trajectory optimization using convex programming and a homotopic approach," *IEEE Transactions on Aerospace and Electronic Systems*, vol. 58, no. 3, pp. 2103–2116, 2022.
- [10] D. Kim, J. D. Turner, and J. L. Junkins, "Optimal actuator failure control using a homotopy method," *Journal of Guidance, Control, and Dynamics*, vol. 38, no. 4, pp. 623–630, 2015.
- [11] G. Liu, W. Feng, K. Yang, and J. Zhao, "Hybrid qpso and sqp algorithm with homotopy method for optimal control of rapid cooperative rendezvous," *Journal of Aerospace Engineering*, vol. 32, no. 4, p. 137, 2019
- [12] L. Cheng, Z. Wang, Y. Song, and F. Jiang, "Real-time optimal control for irregular asteroid landings using deep neural networks," *Acta Astronautica*, vol. 170, no. 3, pp. 66–79, 2020.
- [13] A. Olivier and C. Pouchol, "Combination of direct methods and homotopy in numerical optimal control: Application to the optimization of chemotherapy in cancer," *Journal of Optimization Theory and Applications*, vol. 181, no. 2, pp. 479–503, 2019.
- [14] B. Pan, X. Pan, and Y. Ma, "A quadratic homotopy method for fuel-optimal low-thrust trajectory design," *Proceedings of the Institution of Mechanical Engineers, Part G: Journal of Aerospace Engineering*, vol. 233, no. 5, pp. 1741–1757, 2019.
- [15] X. Pan and B. Pan, "Practical homotopy methods for finding the best minimum-fuel transfer in the circular restricted three-body problem," *IEEE Access*, vol. 8, pp. 47845–47862, 2020.
- [16] R. N. Bergman, L. S. Phillips, and C. Cobelli, "Physiologic evaluation of factors controlling glucose tolerance in man: Measurement of insulin sensitivity and beta-cell glucose sensitivity from the response to intravenous glucose," *The Journal of clinical investigation*, vol. 68, no. 6, pp. 1456–1467, 1981.
- [17] S. Nandi and T. Singh, "Global sensitivity analysis on the bergman minimal model," *IFAC-PapersOnLine*, vol. 53, no. 2, pp. 16112– 16118, 2020.
- [18] M. Nevo-Shenker and S. Shalitin, "The impact of hypo- and hyperglycemia on cognition and brain development in young children with type 1 diabetes," *Hormone Research in Paediatrics*, vol. 94, no. 3-4, pp. 115–123, 2021. [Online]. Available: https://doi.org/10.1159/000517352